


Exploring the cosmological dark matter coincidence using infrared fixed points

Alexander C. Ritter^{✉*} and Raymond R. Volkas^{✉†}

*ARC Centre of Excellence for Dark Matter Particle Physics, School of Physics,
The University of Melbourne, Victoria 3010, Australia*

 (Received 26 October 2022; accepted 3 January 2023; published 31 January 2023)

The asymmetric dark matter (ADM) paradigm is motivated by the apparent coincidence between the cosmological mass densities of visible and dark matter, $\Omega_{\text{DM}} \simeq 5\Omega_{\text{VM}}$. However, most ADM models only relate the number densities of visible and dark matter, and do not motivate the similarity in their particle masses. One exception is a framework introduced by Bai and Schwaller, where the dark matter is a confined state of a dark QCD-like gauge group, and the confinement scales of visible and dark QCD are related by a dynamical mechanism utilizing infrared fixed points of the two gauge couplings. We build upon this framework by properly implementing the dependence of the results on the initial conditions for the gauge couplings in the UV. We then reassess the ability of this framework to naturally explain the cosmological mass density coincidence, and find a reduced number of viable models. We identify features of the viable models that allow them to naturally relate the masses of the dark baryon and the proton while also avoiding collider constraints on the new particle content introduced.

DOI: [10.1103/PhysRevD.107.015029](https://doi.org/10.1103/PhysRevD.107.015029)

I. INTRODUCTION

Determining the particle nature of dark matter (DM) is one of the deepest tasks facing particle physics today. This goal is hampered by the purely gravitational nature of the observational evidence for DM, which has allowed for a cornucopia of DM candidates to be proposed over a wide range of mass scales [1]. To focus our model-building pursuits, it is instructive to see what clues may lie in the existing astrophysical observations.

One such result is the similarity between the present-day cosmological mass densities of dark and visible matter (VM), which we refer to as the *cosmological coincidence* [2]:

$$\Omega_{\text{DM}} \simeq 5\Omega_{\text{VM}}, \quad (1)$$

where Ω_X is the mass density ρ_X for species X divided by the critical density ρ_c .

We take the cosmological coincidence to be a hint towards an underlying link between the origins of the abundances of VM and DM. Such a connection is not

present in the majority of prominent DM candidates. Consider, for example, the weakly interacting massive particle: it is a GeV–TeV scale thermal relic species with an abundance generated through thermal freeze-out. This stands in contrast to VM, whose number density is due to the baryon asymmetry of the Universe and whose mass arises from the confinement energy of QCD. With such distinct generation mechanisms, there is no *a priori* reason why the cosmological mass densities of these species should be of the same order of magnitude.

The main model-building paradigm that seeks to explain the cosmological coincidence problem is that of asymmetric dark matter (ADM) [3,4]. In this framework, the dark matter candidate is charged with a dark particle number that develops an asymmetry related to the visible baryon asymmetry. Models of ADM thus naturally generate similar number densities for VM and DM, $n_{\text{VM}} \sim n_{\text{DM}}$. However, as a mass density is given by $\Omega_X = n_X m_X / \rho_c$, to satisfactorily explain the cosmological coincidence problem we must also motivate the similarity in the particle masses of VM and DM, $m_{\text{VM}} \sim m_{\text{DM}}$. This problem is not addressed in the majority of the ADM literature, which mostly treats the DM mass as a free parameter and thus merely shifts the cosmological mass-density coincidence to a particle mass coincidence.

Our goal then is to construct a theory where DM and VM naturally have similar particle masses. By analogy with the proton, this leads us to consider DM candidates that are confined states of a dark, QCD-like gauge group [5–25], where some mechanism is present to relate the confinement

*Corresponding author.
rittera@student.unimelb.edu.au
†raymondv@unimelb.edu.au

Published by the American Physical Society under the terms of the Creative Commons Attribution 4.0 International license. Further distribution of this work must maintain attribution to the author(s) and the published article's title, journal citation, and DOI. Funded by SCOAP³.

scale Λ_{dQCD} of this gauge group to that of visible QCD, Λ_{QCD} .

Previous efforts to relate the visible and dark confinement scales have followed one of two general directions:

- (1) Introduce a symmetry between the gauge groups. This generally leads to models of mirror matter, where the mirror symmetry is either exact [5–9] or judiciously broken [10–22]. (For other models of mirror matter, see Refs. [26–35].)
- (2) Introduce new field content so that the running gauge couplings α_s and α_d approach infrared fixed points with similar magnitudes. This has not been widely discussed in the literature, with the original idea introduced by Bai and Schwaller [24] and expanded upon by Newstead and TerBeek [25].

In this paper we focus on the latter approach, developing upon the framework introduced by Bai and Schwaller by properly implementing the dependence of the confinement scale Λ_{dQCD} on the initial values of the running gauge couplings in the UV, α_s^{UV} and α_d^{UV} . We then ask how readily this approach generates confinement scales of the same order of magnitude, and so reassess the validity of this framework as a natural explanation of the cosmological coincidence.

Compared to the work of Bai and Schwaller, we find that in our analysis there are a smaller number of models that naturally generate similar confinement scales for visible and dark QCD (dQCD), where models in this framework are defined by the new field content we introduce. This reduced set of models is due to our definition of “naturalness” now being more stringent, as it must take into account the dependence of the dark confinement scale on the initial gauge coupling values in the UV.

In general, we find that models whose infrared fixed points have small values for the gauge couplings are better at generically generating similar visible and dark confinement scales. However, we also find that these models generally require the mass scale of the new particle content to be sub-TeV for most selections of the initial couplings in the UV, and thus are subject to strong collider constraints.

Looking for models where the new physics mass scale is on the order of a few TeV, we do find a number of such models that can fairly generically generate related visible and dark confinement scales. We identify these models as the most promising candidates within this framework for naturally explaining the cosmological coincidence problem.

The paper is organized as follows. In Sec. II we describe the dark QCD framework of Bai and Schwaller. In Sec. III we describe the threshold corrections to the running of the gauge couplings as implemented by Newstead and TerBeek. In Sec. IV we analyze the effect of the values of the gauge couplings in the UV on Λ_{dQCD} . In Sec. V we discuss the ability of this framework to explain the cosmological coincidence, before presenting our results in Sec. VI and concluding in Sec. VII.

TABLE I. New particle content in a model. The given multiplicities are for Dirac fermions and complex scalars. A subscript containing l (h) indicates a multiplicity for light (heavy) particles in cases where this is a relevant distinction to make.

Field	$SU(3)_{\text{QCD}} \times SU(3)_{\text{dQCD}}$	Mass	Multiplicity
Fermion	(3, 1)	M	$n_{f_{c,h}}$
	(1, 3)	$< \Lambda_{\text{dQCD}}$	$n_{f_{d,l}}$
	(3, 3)	M	$n_{f_{d,h}}$
	(3, 3)	M	n_{f_j}
Scalar	(3, 1)	M	n_{s_c}
	(1, 3)	M	n_{s_d}
	(3, 3)	M	n_{s_j}

II. BAI-SCHWALLER FRAMEWORK

The scheme of Bai and Schwaller [24] utilizes a dark QCD-like gauge group $SU(N_d)_{\text{dQCD}}$, along with a selection of new particle content charged under $SU(3)_{\text{QCD}} \times SU(N_d)_{\text{dQCD}}$. As in the original paper, we only consider $N_d = 3$, and limit the new field content to fermions and scalars in the fundamental representations of either one or both of the QCD gauge groups.¹ The multiplicities of the new particles are given in Table I, along with their masses. In addition to the given multiplicities, we also define $n_{f_d} = n_{f_{d,h}} + n_{f_{d,l}}$ as the total number of dark fermion species that are fundamentals of $SU(3)_{\text{dQCD}}$, and $n_{f_c} = n_{f_{c,h}} + 6$ as the multiplicity of visible fermions that are fundamentals of $SU(3)_{\text{QCD}}$ [including the six Standard Model (SM) quarks].

The majority of the new field content is, for simplicity, taken to exist at a common heavy mass scale M , except for the $n_{f_{d,l}}$ light dark fermions. These latter particles, which we refer to as “dark quarks,” have masses much lighter than the dark confinement scale Λ_{dQCD} and are confined into the dark baryons that serve as the DM candidate.

At the two-loop level, the β functions for g_c and g_d are coupled, thanks to the presence of the “joint” fields charged under both $SU(3)_{\text{QCD}}$ and $SU(3)_{\text{dQCD}}$. The two-loop β function for g_c , $\beta_c(g_c, g_d) = \frac{dg_c}{d(\log(\mu))}$, is given by

$$\begin{aligned} \beta_c = & \frac{g_c^3}{16\pi^2} \left[\frac{2}{3}(n_{f_c} + 3n_{f_j}) + \frac{1}{6}(n_{s_c} + 3n_{s_j}) - 11 \right] \\ & + \frac{g_c^5}{(16\pi^2)^2} \left[\frac{38}{3}(n_{f_c} + 3n_{f_j}) + \frac{11}{3}(n_{s_c} + 3n_{s_j}) - 102 \right] \\ & + \frac{g_c^3 g_d^2}{(16\pi^2)^2} [8n_{f_j} + 8n_{s_j}], \end{aligned} \quad (2)$$

¹While we do not address the possibility here, one could also consider models with $N_d \neq 3$. We would anticipate qualitatively different results, as changing N_d alters a number of aspects of the framework; the selections of field content that result in an infrared fixed point would differ, as would the running of the dark gauge coupling after the new physics has decoupled.

and the β function for g_d , $\beta_d(g_c, g_d) \equiv \frac{dg_d}{d(\log(\mu))}$, is obtained by exchanging the indices $c \leftrightarrow d$ [36]. Note that these β functions are given for $N_c = N_d = 3$; the β functions for general N_c and N_d can be found in Ref. [24].

Depending on the particle content, there may be nontrivial couplings α_s^* and α_d^* for which both β functions are zero, where $\alpha_s = g_c^2/4\pi$, $\alpha_d = g_d^2/4\pi$, and

$$\beta_c(g_c^*, g_d^*) = \beta_d(g_c^*, g_d^*) = 0. \quad (3)$$

The couplings α_s^* and α_d^* denote an infrared fixed point (IRFP) of the renormalization group running similar to a Banks-Zaks fixed point for a single gauge coupling [37]. The couplings at the IRFP only depend on the multiplicities of the new particle content, $(n_{f_{c,h}}, n_{f_{d,l}}, n_{f_{d,h}}, n_{f_j}, n_{s_c}, n_{s_d}, n_{s_j})$; we refer to a given selection of multiplicities as a “model.”

So, for a given model, if there exists a nontrivial perturbative IRFP, the coupled gauge couplings evolve toward α_s^* and α_d^* regardless of the initial values for the gauge couplings in the UV. This fixed-point feature is broken when the new heavy fields decouple at the mass scale M ; below this scale, the gauge couplings run independently until they become nonperturbative at the confinement scales Λ_{QCD} and Λ_{dQCD} .

The process to calculate Λ_{dQCD} for a given model is then, ideally, as follows:

- (1) Calculate the IRFP gauge couplings α_s^* and α_d^* .
- (2) Determine M by running the visible coupling up from the measured value $\alpha_s(M_Z) = 0.11729$ [38] to $\alpha_s(M) = \alpha_s^*$.
- (3) Evolve the dark coupling down from $\alpha_d(M) = \alpha_d^*$ until the scale Λ_{dQCD} at which it becomes large enough to trigger confinement. As a rough perturbative condition, the Cornwall-Jackiw-Tomboulis bound $\alpha_s > \pi/4$ for $N_d = 3$ [39] is used to define the dark confinement scale through $\alpha_d(\Lambda_{\text{dQCD}}) = \pi/4$.

So, for a given model with a nontrivial IRFP, the dark confinement scale Λ_{dQCD} can be uniquely determined. The argument is then that a model with related IRFP values α_s^* and α_d^* could lead to compatible confinement scales for visible and dark QCD of similar orders of magnitude.

However, this framework relies upon a number of simplifying assumptions that should be investigated in greater detail. The first is that the heavy fields decouple at the mass scale M without any threshold corrections, which was addressed in Ref. [25]; we summarize their approach in the next section. The second key assumption is that the couplings run all the way to their IRFP values by the decoupling scale M regardless of the initial coupling values in the UV. However, this is not true in general, and in a later section we analyze how the value of Λ_{dQCD} depends on the UV coupling values α_s^{UV} and α_d^{UV} .

III. THRESHOLD CORRECTIONS

In minimal subtraction like mass-independent renormalization schemes, the Appelquist-Carazzone decoupling theorem [40] does not apply in its naive form; heavy fields can continue to influence coupling constants and β functions at energy scales below their masses. In these schemes there also arises the related issue of large logarithms when working at energy scales much smaller than the mass M of the heavy fields.

To properly account for these problems, the decoupling is treated explicitly by constructing an effective field theory (EFT) in which the heavy fields have been integrated out. Consistency is ensured by matching the full theory onto the effective field theory at a matching scale μ_0 , where $\mu_0 \sim M$ to avoid large logarithms. This procedure leads to a “consistency condition” relating the coupling constants in the full theory with the coupling constants in the effective field theory [41,42],

$$\alpha_s^{\text{EFT}}(\mu_0) = \zeta_c^2(\mu_0, \alpha_s(\mu_0))\alpha_s(\mu_0), \quad (4)$$

$$\alpha_d^{\text{EFT}}(\mu_0) = \zeta_d^2(\mu_0, \alpha_d(\mu_0))\alpha_d(\mu_0). \quad (5)$$

The decoupling functions ζ_c^2 and ζ_d^2 have been determined to three- and four-loop order in Refs. [43,44] for the case of integrating out one heavy quark from QCD with n_f flavors. Since we are working with two-loop β functions, we only require the one-loop decoupling functions; in Ref. [25], the results of Ref. [43] were adapted for integrating out the full selection of heavy field content at mass M , with the one-loop decoupling functions given by

$$\zeta_c^2(\mu, \alpha_s(\mu)) = 1 - \frac{\alpha_s(\mu)}{6\pi} \tilde{n}_c \log\left(\frac{\mu^2}{M^2}\right), \quad (6)$$

$$\zeta_d^2(\mu, \alpha_d(\mu)) = 1 - \frac{\alpha_d(\mu)}{6\pi} \tilde{n}_d \log\left(\frac{\mu^2}{M^2}\right), \quad (7)$$

where the coefficients \tilde{n}_c and \tilde{n}_d account for the degrees of freedom of the relevant heavy fields,

$$\tilde{n}_c = n_{f_{c,h}} + 3n_{f_j} + \frac{1}{4}(n_{s_c} + 3n_{s_j}), \quad (8)$$

$$\tilde{n}_d = n_{f_{d,h}} + 3n_{f_j} + \frac{1}{4}(n_{s_d} + 3n_{s_j}). \quad (9)$$

We note that, for a given M , the values of the couplings at low energies now depend on the choice of decoupling scale μ_0 ; this renormalization scale dependence is a nonphysical artifact of our perturbative analysis being truncated at finite loop order. As a result, the procedure of Bai and Schwaller [matching $\alpha_s(M_Z)$ to its experimental value] no longer uniquely determines the value of M when we incorporate the threshold corrections to the coupling constants. Instead,

we obtain a relationship between M and μ_0 , and can solve for one of these values if we specify the other.

In Ref. [25], values of Λ_{dQCD} were determined for a given model and value of M . By using the consistency condition and again matching the strong coupling to its measured value at M_Z , they solved for the decoupling scale μ_0 , and then ran the dark coupling until $\alpha_d(\Lambda_{\text{dQCD}}) = \pi/4$. However, this process does not ensure that μ_0 is on the order of M . We take a different approach to implementing threshold corrections, as is detailed in the following section.

IV. DEPENDENCE ON INITIAL UV COUPLINGS

As mentioned earlier, the framework in the previous sections assumes that the couplings run to their IRFP values by the decoupling scale μ_0 regardless of their initial values in the UV, α_s^{UV} and α_d^{UV} . However, this is not the case, as illustrated in Fig. 1 for the model $(n_{f_{c,h}}, n_{f_{d,l}}, n_{f_{d,h}}, n_{f_j}, n_{s_c}, n_{s_d}, n_{s_j}) = (0, 3, 3, 3, 3, 2, 0)$ with IRFP $(\alpha_s^*, \alpha_d^*) = (0.045, 0.077)$, where we show the running of a grid of couplings (α_s, α_d) from the UV scale $\Lambda_{\text{UV}} = 10^{19}$ GeV down to a typical infrared scale $\Lambda_{\text{IR}} = 1$ TeV. While the couplings evolve towards their fixed-point values, they do not precisely reach them, and so the low-energy behavior of the theory exhibits some dependence on the couplings in the UV.

We now account for this dependence in our calculation of Λ_{dQCD} . Consider the running of the couplings in this model for a given mass scale M and initial UV couplings $(\alpha_s^{\text{UV}}, \alpha_d^{\text{UV}})$. The couplings evolve with the full coupled renormalization group equations (RGEs) until the scale μ_0 at which we apply the matching conditions of Eqs. (4) and (5). Unlike the approach of Ref. [25], we explicitly ensure that $\mu_0 \sim \mathcal{O}(M)$; following the approach of Refs. [44,45], we vary μ_0 between $0.5M$ and $2M$ and treat the variance in

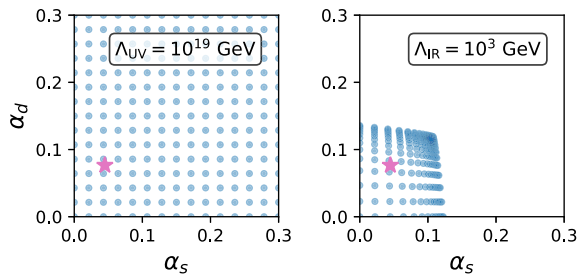


FIG. 1. Left: a grid of values for the strong coupling constant α_s and the dark coupling constant α_d at an energy scale $\Lambda_{\text{UV}} = 10^{19}$ GeV. The pink star shows the infrared fixed point $(\alpha_s^*, \alpha_d^*) = (0.045, 0.077)$ for the model with field multiplicities $(n_{f_{c,h}}, n_{f_{d,l}}, n_{f_{d,h}}, n_{f_j}, n_{s_c}, n_{s_d}, n_{s_j}) = (0, 3, 3, 3, 3, 2, 0)$. Right: the grid of values from the left panel is evolved down from 10^{19} GeV to an energy scale $\Lambda_{\text{IR}} = 10^3$ GeV under the RGEs of the given model. The pink star again indicates the IRFP of the model.

the low-energy running of the couplings as a theoretical uncertainty due to working at finite loop order.² This then leads to an uncertainty in the value of Λ_{dQCD} . This evolution is depicted in Fig. 2, where the blue band shows the possible range of Λ_{dQCD} values for this given model, mass scale M and initial UV couplings.

The process for calculating Λ_{dQCD} for a given model is now as follows:

- (1) We first specify the UV couplings $(\alpha_s^{\text{UV}}, \alpha_d^{\text{UV}})$; we then determine the required decoupling scale μ_0 by solving Eq. (4) where $\alpha_s^{\text{EFT}}(\mu_0)$ is given by running the visible coupling up from $\alpha_s^{\text{EFT}}(M_Z) = 0.11729$ and $\alpha_s(\mu_0)$ is given by running $(\alpha_s^{\text{UV}}, \alpha_d^{\text{UV}}) \rightarrow (\alpha_s(\mu_0), \alpha_d(\mu_0))$.
- (2) However, this does not uniquely specify μ_0 , as the decoupling function ζ_c^2 depends on M . Since ζ_c^2 depends on M through the factor $\log(\mu^2/M^2)$, we can solve for μ_0 (and also for M) by specifying a value for μ_0/M .
- (3) To account for the uncertainty introduced by threshold corrections, we vary the value of μ_0/M between 0.5 and 2. This results in a range of values for M for the given pair of initial UV couplings.
- (4) We then calculate Λ_{dQCD} as usual by running $\alpha_d^{\text{EFT}}(\mu_0)$ to $\alpha_d^{\text{EFT}}(\Lambda_{\text{dQCD}}) = \pi/4$. Since there is a range of possible values for M (and thus μ_0), we also obtain a range of values for Λ_{dQCD} .

We note that this process will not work for all pairs of UV couplings, as we require the low-energy running of α_s to match with experiment. This matching is performed by solving for the decoupling scale such that α_s reaches its measured value at M_Z , and for some initial UV couplings, there will be no value of the new physics mass scale M between M_{Pl} and M_Z for which this occurs.

With this process specified, we are interested in how Λ_{dQCD} depends on the initial UV couplings for a given model. As an example, in Fig. 3 we plot contours of Λ_{dQCD} on axes of α_s^{UV} against α_d^{UV} , where we work with perturbative couplings between 0 and 0.3 to ensure that we can trust our two-loop β -function calculations.³ We see that

²References [44,45] applied this approach to the running of α_s across quark thresholds in the SM between m_τ and M_Z . For a quark of mass m_q , they varied the decoupling scale between $0.7m_q$ and $3m_q$; however, since this process is intended to minimize large logarithms, we chose to vary the decoupling scale between multiplicatively symmetric values around M . Regardless of the specific choice made, note that this is merely a simple, arbitrary condition which roughly captures the uncertainty in the decoupling of the heavy fields. Indeed, other more sophisticated schemes have been developed to minimize the effect of unphysical renormalization-scale dependence in threshold corrections (see for example Refs. [46–48]) but these are beyond the scope of this analysis.

³We discuss this choice for the range of initial UV couplings in greater detail in Sec. VA.

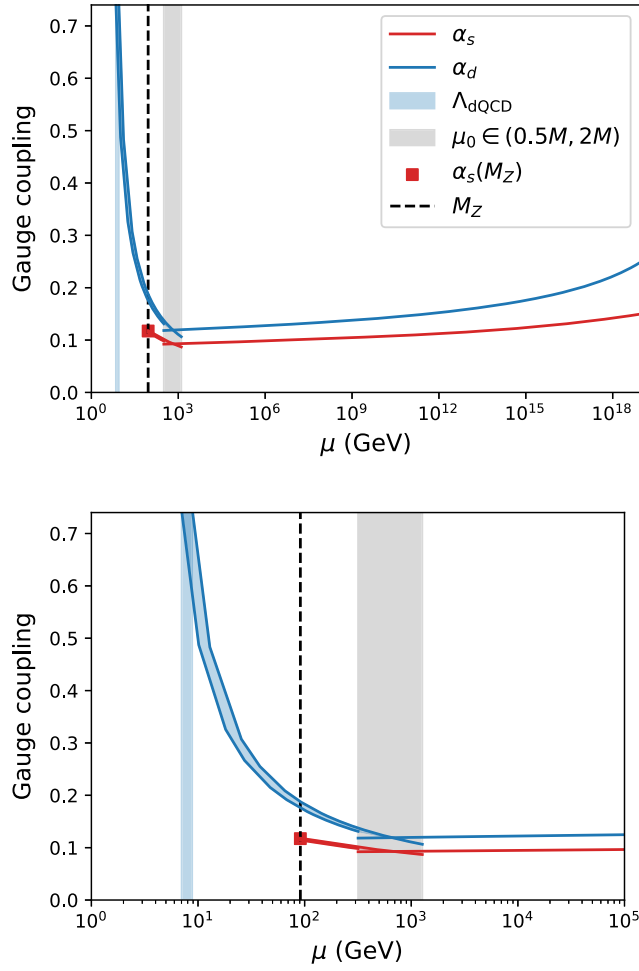


FIG. 2. Top: the evolution of the QCD and dQCD coupling constants for the model $(n_{f_{c,h}}, n_{f_{d,l}}, n_{f_{d,h}}, n_{f_j}, n_{s_c}, n_{s_d}, n_{s_j}) = (0, 3, 3, 3, 3, 2, 0)$ with mass scale $M = 635$ GeV and initial UV couplings $(\alpha_s^{\text{UV}}, \alpha_d^{\text{UV}}) = (0.15, 0.25)$. The mass scale is chosen so that α_s obtains its measured value at M_Z , as indicated by the red square. The decoupling scale μ_0 is shown by the grey shaded band, where we allow it to vary between $0.5M$ and $2M$ to account for the uncertainty introduced by threshold corrections. Below the decoupling scale, α_s and α_d are depicted as bands, due to the variance in the decoupling scale. The vertical blue band indicates the range of values for the dark confinement scale Λ_{dQCD} , calculated as the energy scale where $\alpha_d = \pi/4$. Bottom: the same evolution, zoomed in to the energy range between 1 and 10^5 GeV to show the variance in the coupling constants below the decoupling scale more clearly.

Λ_{dQCD} is larger for small values of α_s^{UV} , and is smaller for small values of α_d^{UV} . Note that the contours are in fact shaded bands to account for the uncertainty in Λ_{dQCD} ; however, the threshold corrections do not have a drastic effect, as the bands are fairly narrow.

In Fig. 3 we also show contours for the required new physics mass scale M , which increases as α_s^{UV} decreases. In the red hatched areas there are no allowed values of M for which α_s has the correct running at low energy.

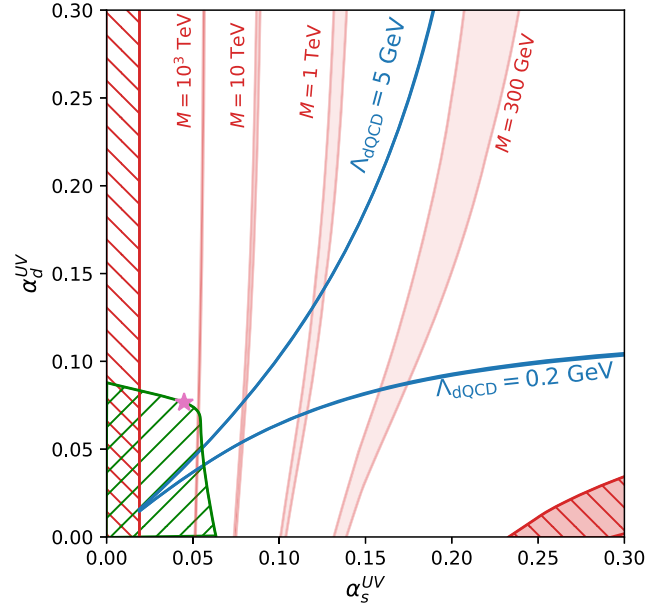


FIG. 3. For the model $(n_{f_{c,h}}, n_{f_{d,l}}, n_{f_{d,h}}, n_{f_j}, n_{s_c}, n_{s_d}, n_{s_j}) = (0, 3, 3, 3, 3, 2, 0)$ we show contours for the dark confinement scale Λ_{dQCD} (blue) and for the new physics scale M (red) on axes of the initial UV couplings α_s^{UV} and α_d^{UV} . The width of these contours is due to the variance in the decoupling scale μ_0 between $0.5M$ and $2M$ to account for the uncertainty introduced by threshold corrections. In the red hatched regions there are no allowed values of M for which α_s has the correct running at low energy. The pink star shows the infrared fixed point of this model. The green hatched region is the “asymptotically free” region, where $SU(3)_{\text{QCD}}$ and $SU(3)_{\text{dQCD}}$ both exhibit asymptotic freedom.

A. Asymptotic freedom

In Fig. 3 we also include a star and a green hatched region. The star indicates the coupling values at the IRFP, and the green hatched region shows the “asymptotically free” region, that is, the region of the perturbative $(\alpha_s^{\text{UV}}, \alpha_d^{\text{UV}})$ parameter space for which $SU(3)_{\text{QCD}}$ and $SU(3)_{\text{dQCD}}$ both exhibit asymptotic freedom.

It is an interesting consequence of the existence of a nontrivial IRFP with coupled β functions that the asymptotic freedom of the theory depends upon the values of the two gauge couplings. The intuition for this observation is as follows: as the energy scale approaches the IR, the gauge couplings approach their IRFP values, which we can also think of as points in the (α_s, α_d) parameter space running toward the IRFP. So, as the energy scale approaches the UV, all points in the parameter space evolve away from the IRFP. There is a UV fixed point at the origin, $\alpha_s = \alpha_d = 0$; points that are roughly “closer” to the origin than the IRFP evolve towards this fixed point and thus both visible and dark QCD will exhibit asymptotic freedom. Those points “further away” from the origin than the IRFP instead diverge toward large couplings and do not exhibit asymptotic freedom.

To see this region more concretely, we treat the β functions as a vector field describing the flow of the

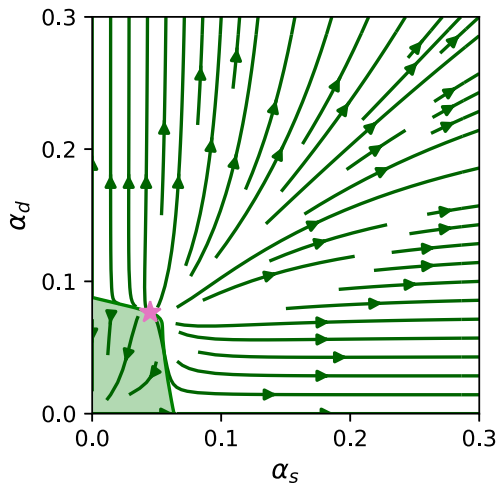


FIG. 4. A streamline plot for the vector field defined by the coupled β functions for α_s and α_d for the model $(n_{f_{c,h}}, n_{f_{d,d}}, n_{f_{d,h}}, n_{f_j}, n_{s_c}, n_{s_d}, n_{s_j}) = (0, 3, 3, 3, 3, 2, 0)$, where the green arrows indicate the change in the coupling constants with increasing energy scale μ . The shaded green region is the “asymptotically free” region, corresponding to the green hatched region in Fig. 3. Within this region, both coupling constants approach zero as the energy scale increases. The pink star shows the infrared fixed point of this model.

couplings with increasing energy scale and plot its streamlines in Fig. 4. We can clearly see the qualitative behavior described in the previous paragraph, along with the edge of the asymptotically free region as shown in Fig. 3.

We note that although we have identified the region of (α_s, α_d) parameter space for which the gauge groups are not asymptotically free, we do not discount this region. Since we work with α_s^{UV} and α_d^{UV} below 0.3, we only consider running in which the couplings are perturbative up to the Planck scale. Thus, dynamics at energies above the Planck scale may change the running again and regain asymptotic freedom or create a nonzero UV fixed point as per the “asymptotic safety” idea [49,50].

V. EXPLAINING THE COSMOLOGICAL COINCIDENCE PROBLEM

Now that we have accounted for the dependence of Λ_{dQCD} on the initial UV couplings, in this section we reassess whether this framework offers a natural solution to the cosmological coincidence problem.

To “solve” the cosmological coincidence problem, we mean that we want our theory to naturally generate a mass density Ω_{DM} on the order of Ω_{VM} . In this work we focus only on explaining the similarity between the particle masses, $m_{\text{VM}} \sim m_{\text{DM}}$, and do not specify the ADM mechanism through which the number densities are related.⁴ We assume

⁴For an example of an ADM mechanism that can be implemented in this framework, see the leptogenesis model of Ref. [24].

that the ADM mechanism generates similar number densities $n_{\text{VM}} \sim n_{\text{DM}}$, and also assume that the relationship between the baryon mass and confinement scale is the same for both visible and dark QCD. Then, to satisfy Eq. (1), we need a dark confinement scale $\Lambda_{\text{dQCD}} \sim 1$ GeV. We let this vary by a factor of 5 to approximately account for different dynamical completions that would be expected to produce a range of reasonable values for the $n_{\text{VM}}/n_{\text{DM}}$ ratio. So, we define a “valid” value of Λ_{dQCD} to be between 0.2 and 5 GeV.

We now need to determine how “natural” this framework is, that is, how readily it generates valid values for Λ_{dQCD} . We consider the theory to provide a natural explanation of the coincidence problem if one obtains a valid Λ_{dQCD} value for a large proportion of the available parameter space, as we do not wish for the cosmological coincidence to arise from any fine-tuning of the parameters.

Of course, an ambiguity arises in the notion of “available” parameter space. The parameters we vary are the multiplicities of the field content and the initial values of the couplings in the UV; clearly, we must place some restrictions on these parameters when searching for valid Λ_{dQCD} values, both to provide a finite space in which to look and to avoid considering unphysical theories. So, the question we ask of the theory is as follows: given a certain set of assumptions, is it a surprise that we obtain a valid value for the dark confinement scale?

In this section we do not argue for a unique set of such assumptions; rather, we discuss a number of assumptions one could make, and give freedom to the reader to place their own set of requirements on the theory when assessing its validity. We then present a set of results given only a minimal set of assumptions, and highlight features of the theory that affect how readily it obtains a valid dark confinement scale.

A. Assessing the validity of a given model

We start this discussion by considering a given model, where we fix the multiplicities of the new fields as given in Table I. This specifies the IRFP and the β functions, but leaves us free to vary the initial UV couplings α_s^{UV} and α_d^{UV} . The question then is what assumptions we place on the selection of these initial UV couplings; in particular, what range of values do we select our couplings from, and how do we randomly select coupling values from this range?

To answer this question requires knowledge of the inaccessible dynamics above the Planck scale that generate the values of these parameters at the UV scale. We must remain agnostic to these dynamics, and so the simplest assumption we apply is that the gauge couplings are perturbative at the UV scale, that is, both α_s^{UV} and α_d^{UV} lie between 0 and 1.

However, as seen in Figs. 1 and 3, we chose to work with initial UV couplings that lie between 0 and 0.3. This is done to ensure the perturbative validity of our two-loop β function calculations. From Eq. (2), and recalling that

$\alpha = g^2/4\pi$, we see that the individual one- and two-loop nongluonic terms that contribute to the β functions—which we call $\beta^{(1)}$ and $\beta^{(2)}$, respectively—are of the form

$$\beta^{(1)} \sim \frac{\alpha^2 n}{2\pi}, \quad \beta^{(2)} \sim 20 \frac{\alpha^3 n}{8\pi^2}, \quad (10)$$

where n is a multiplicity, and the factor of ~ 20 accounts for the relative size of the numerical coefficients for the one- and two-loop terms, due to various group-theoretic factors. Then, to ensure that the individual two-loop terms are smaller than the individual one-loop terms implies the rough condition $\alpha_s, \alpha_d < 0.3$. From now on, we refer to gauge couplings smaller than 0.3 as “perturbative” couplings, in the stricter sense that both the couplings themselves are perturbative, and that the β functions governing their RGE running admit a perturbative analysis.

Other restrictions we could place on α_s^{UV} and α_d^{UV} depend upon how strongly we require a given model to replicate our Universe. For example, one could discount points in the red hatched regions of Fig. 3 where there is no value of the new physics scale M for which the low-energy running of α_s matches with experiment. However, one could argue that a given model is equally theoretically valid with any perturbative values for the initial UV couplings; the fact that the model fails this phenomenological test for certain initial UV couplings is just one way in which it is unable to obtain a valid value for the dark confinement scale. Put another way, the difference is between asking the following questions:

- (1) “Given that our model has perturbative values for α_s^{UV} and α_d^{UV} , how likely is it that we replicate the low-energy running of α_s and also obtain a valid value for the dark confinement scale?”
- (2) “Given that our model has perturbative values for α_s^{UV} and α_d^{UV} and replicates the low-energy running of α_s , how likely is it that we obtain a valid value for the dark confinement scale?”

For the results we present in Sec. VI, we take the first of these approaches when analyzing a given model.

Another possible assumption of this type is to only consider UV couplings for which the required value of M is on the order of a TeV or greater, as new sub-TeV color-charged particles would be produced readily at colliders.

For a given model, one could also choose to only work with UV couplings for which the model is truly asymptotically free. However—as discussed in Sec. IVA—given that we only consider α_s^{UV} and α_d^{UV} with values smaller than 0.3, there will be no Landau poles below the Planck scale. Above the Planck scale, unknown physics could cause these models to regain asymptotic freedom or achieve asymptotic safety, so it is valid to consider such points.

The last point to consider here is the process by which we randomly select values for α_s^{UV} and α_d^{UV} from a specified range. This again requires knowledge of physics

above the Planck scale; given our lack of knowledge, we make the simple assumption that the couplings are selected uniformly randomly between 0 and 0.3 for each coupling.

Given the simplest of these assumptions, we define the “validity fraction” ϵ_v to be the fraction of the UV coupling parameter space— $0 < \{\alpha_s^{\text{UV}}, \alpha_d^{\text{UV}}\} < 0.3$ —that lies between the 0.2 and 5 GeV contours for Λ_{dQCD} . This is roughly the likelihood that a given model will obtain a valid value of Λ_{dQCD} given a random choice of perturbative initial UV couplings. As an approximate condition, we consider models with large values of ϵ_v to be those that explain the cosmological coincidence problem. The definition of a “large” value of ϵ_v is, of course, subjective to some extent, and we shall see what constitutes the largest possible values of ϵ_v when we present results in Sec. VI.

B. Assessing the validity of the framework

Now that we have discussed the assumptions one could make to assess the validity of a given model, we can look at how readily the overall framework can serve as an explanation of the coincidence problem. That is, within the space of all possible models (as defined by the multiplicities of the new fields we introduce), how many of them provide viable explanations of the cosmological coincidence problem? To answer this question, we must look at the assumptions we choose to restrict this space of all possible models.

In Ref. [25], the space of all possible models is set by calculating a “maximum multiplicity” for each new field; these are determined by the requirement that the one-loop terms for β_c and β_d in Eq. (2) remain negative.⁵ For each new field, its maximum multiplicity is calculated assuming that all other new field multiplicities are zero; the resulting values are given in Table II.

Within this total space of possible models, we can apply further restrictions on the set of models we consider. The first, of course, is to consider only those models with a perturbative infrared fixed point. We could also consider only those models whose IRFP satisfies $\alpha_s^* < \alpha_s(M_Z)$ and $\alpha_d^* < \pi/4$. Before accounting for the dependence of the dark confinement scale on the initial UV couplings, this was a necessary condition to apply to a given model to even obtain a dark confinement scale; since the couplings were assumed to take their IRFP values at the decoupling scale, these values must be lower than the values they need to

⁵In Ref. [25], this condition is chosen to ensure that the gauge groups are QCD-like. In our work, we often work with gauge couplings where the models are not asymptotically free, so it is less obvious that we should also require negative one-loop terms in our β functions. However, the existence of an IRFP ensures that there is an asymptotically free region surrounding the origin—as shown in Fig. 4—and to have asymptotic freedom for α_s and α_d close to zero requires that the one-loop terms in the β functions are negative.

TABLE II. The maximum multiplicities for each new field. These are set by the requirement that the one-loop terms for the β functions are negative, which is necessary for the existence of an infrared fixed point.

Multiplicity	$n_{f_{c,h}}$	n_{f_d}	n_{f_j}	n_{s_c}	n_{s_d}	n_{s_j}
Maximum value	10	16	3	42	66	14

reach at low energy after decoupling. However, with our alteration to the framework, there will be initial UV coupling values for which a dark confinement scale can be calculated, even for models whose IRFP values α_s^* and α_d^* are larger than $\alpha_s(M_Z)$ and $\pi/4$, respectively; thus, we are not required to apply this restriction to the models we consider.

VI. RESULTS

In this section we present results using a minimal set of the assumptions discussed in the previous section. We focus on finding models that can viably explain the coincidence problem, and identifying the features of these models that allow them to do so.⁶ To identify these viable models, we use the validity fraction ϵ_v as defined in Sec. VA.

The entire space of possible models, as limited by the maximum field multiplicities of Table II, is too large to search through efficiently. We begin this section by instead looking in detail at a limited set of models, i.e., those that have at most three copies of each new field, as specified by the field identifications in Table I. We also require that $n_{f_{d,i}} \geq 1$, so that there is at least one light dark quark species to confine into the dark baryons. The choice of at most three copies of each field is only to make the set of models more amenable to study; however, these models also would present an easier task if one wished to do further model building and detailed phenomenology with one of them in particular.

A. Analyzing models with $n_i \leq 3$

There are 12 288 total models of this type. Of these, 1354 have an infrared fixed point and 155 have an IRFP for which both couplings are perturbative; recall that we consider a gauge coupling to be perturbative if it is smaller than 0.3, as discussed in Sec. VA. The values of ϵ_v for this set of 155 models are shown in Fig. 5. There are no models for which ϵ_v is greater than 0.4, and there is a tendency towards smaller values of ϵ_v .

⁶While this section focuses on identifying viable models within our expanded framework, in the Appendix we present results for the seven benchmark models from the original work of Bai and Schwaller; this serves as a point of comparison between the new and old analyses.

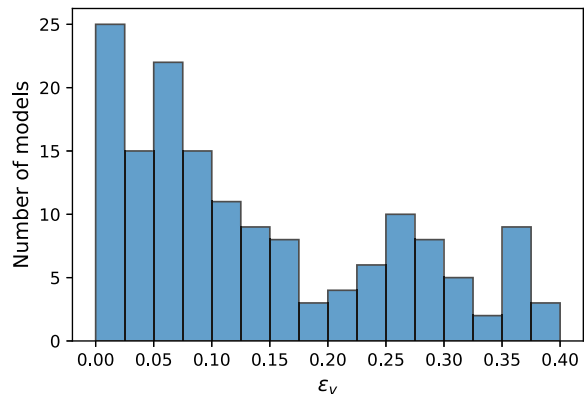


FIG. 5. A histogram of the validity fractions for the set of 155 models that have at most three of each new field and a perturbative IRFP.

We consider models with larger values of ϵ_v to be those that are best able to explain the cosmological coincidence problem; we thus are interested in the features of the models with the largest values of ϵ_v , and so in Fig. 6 we show the 12 models for which $\epsilon_v > 0.35$. Roughly, these are the models for which there is at least a 1 in 3 chance that a randomly chosen pair of perturbative initial UV couplings will generate similar values of the visible and dark confinement scales.

Looking at the Λ_{dQCD} contours for these 12 models, we can first see why there may be no models for which ϵ_v is greater than 0.4. When the initial UV couplings are too dissimilar, we do not obtain a dark confinement scale similar to the visible confinement scale; for smaller α_s^{UV} and larger α_d^{UV} , Λ_{dQCD} is too large, and for smaller α_d^{UV} and larger α_s^{UV} , Λ_{dQCD} is too small. This makes sense: to obtain similar confinement scales for the two gauge groups, their couplings must be similar at the decoupling scale, and so cannot be too different in the UV.

The next observation we make is that all 12 models have small fixed points, with both α_s^* and α_d^* less than 0.1. This correlation between smaller IRFP values and larger validity fractions is clear in Fig. 7, where we plot the IRFPs for the set of 155 models, sized by the value of ϵ_v . The 12 models with $\epsilon_v > 0.35$ are shown in pink, and cluster in a region centred on $\alpha_s^{\text{UV}}, \alpha_d^{\text{UV}} \sim 0.05$.

We can understand easily why larger ϵ_v would correlate with smaller α_s^* . At the decoupling scale, $\alpha_s(\mu_0)$ must be smaller than $\alpha_s(M_Z)$ (whose value is indicated in Fig. 7 with a black dashed line) in order to have the correct low-energy running. So, for this to occur in a decent proportion of the UV coupling parameter space, the couplings must evolve towards a fixed point where α_s^* is smaller than $\alpha_s(M_Z)$. Conversely, when α_s^* is greater than $\alpha_s(M_Z)$, then for many pairs of initial UV couplings with larger values of α_s^{UV} there is no mass scale M for which α_s has the correct low-energy running. This can be seen in Fig. 6 for the

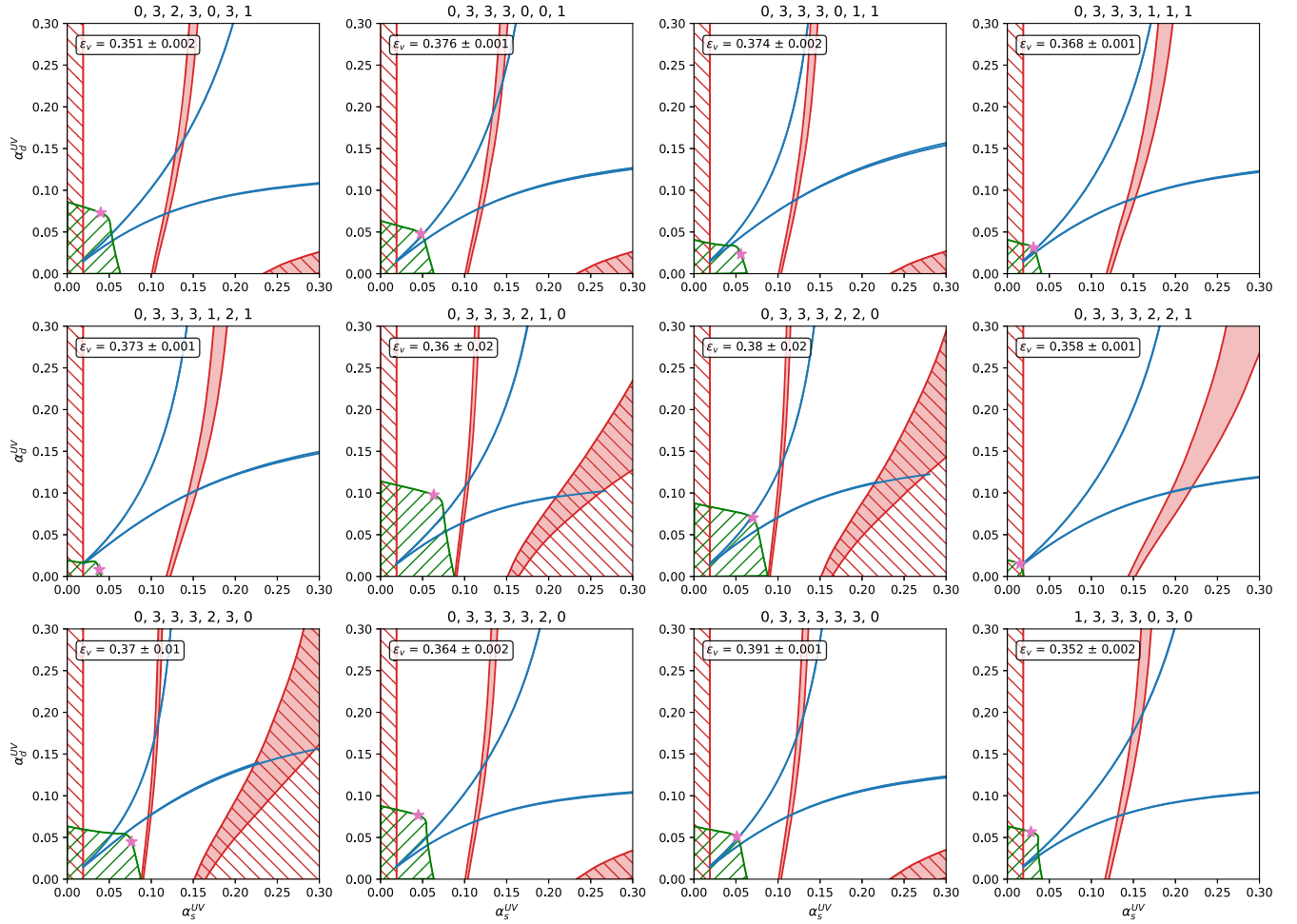


FIG. 6. Each subplot shows the results for a given model on axes of the initial UV couplings, where the plot features are similar to those in Fig. 3. In blue we show the contours for $\Lambda_{\text{dQCD}} = 0.2$ GeV (rightmost contour) and 5 GeV (leftmost contour); the validity fraction ϵ_v is calculated as the proportion of the parameter space between these two contours. In red we show the contour for $M = 1$ TeV, and note that $M > 1$ TeV to the left of the red contour; we also show the red hatched regions where there are no valid values for M . The green hatched region indicates the “asymptotically free” region, and the pink star shows the IRFP of the model. The 12 models shown are those with at most three of each new field, a perturbative IRFP, and a validity fraction $\epsilon_v > 0.35$. The title of each subplot gives the field multiplicities of the given model: $n_{f_{c,h}}, n_{f_{d,l}}, n_{f_{d,h}}, n_{f_j}, n_{s_c}, n_{s_d}, n_{s_j}$.

models with α_s^* closest to 0.1, and is clearer in Fig. 8, where we show the models with the four largest values of α_s^* .

Given that small α_s^* correlates with larger ϵ_v , we can also understand heuristically why α_d^* should also be small in these cases. As mentioned earlier, for the visible and dark confinement scales to be of similar orders of magnitude, α_s and α_d should generally have similar values at the decoupling scale; to achieve this for a decent proportion of the UV coupling parameter space, the couplings should thus be evolving towards a fixed point with similar values for α_s^* and α_d^* .

The last observation we make here is about the size of the new physics scale in these models. In Fig. 6, to the right of the red contour in each plot we have $M < 1$ TeV. This would imply a plethora of new, colored sub-TeV particles, and the model at these parameter points would be ruled out by collider constraints. So, although within our selection of

155 models we have found 12 with a decent validity fraction $\epsilon_v > 0.35$, they would be ruled out by experiment for the majority of their valid parameter space.

Now that we have identified some features of models that correlate with larger values of ϵ_v , we wish to see if we can find models that have a sufficiently large new physics scale M to avoid strong collider constraints in addition to having a large validity fraction.

B. Searching for models with larger M

To find models that have larger scales of new physics, we need to know how M depends upon the selection of field multiplicities.

Recall that M is determined by the requirement that we replicate the low-energy running of α_s : using the consistency condition of Eq. (4), we solve for the decoupling

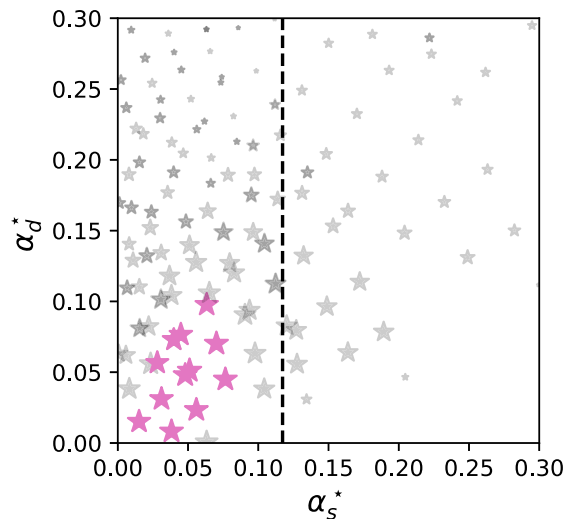


FIG. 7. Each star shows the infrared fixed point of a model, sized by the validity fraction ϵ_v for that model. The set of models shown in this plot are the 155 models with at most three of each new field and a perturbative infrared fixed point. The pink stars correspond to the 12 models with $\epsilon_v > 0.35$ that are shown in Fig. 6. The black dashed line is at $\alpha_s(M_Z) = 0.11729$.

scale μ_0 at which $\alpha_s(\mu_0)$ running under the β functions of the full model matches onto $\alpha_s^{\text{EFT}}(\mu_0)$ given by its SM running from $\alpha_s^{\text{EFT}}(M_Z) = 0.11729$. By specifying a value of $\mu_0/M \in (0.5, 2)$ we can then solve for M .

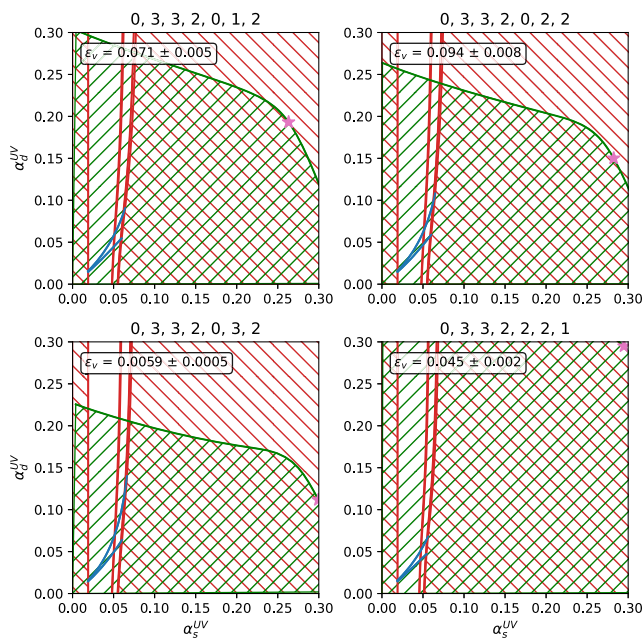


FIG. 8. Results for the four models with the largest values of α_s^* from the set of models with at most three of each new field and a perturbative IRFP. The features of each subplot are the same as those in Fig. 6. Note that a larger value of α_s^* correlates with a larger proportion of the parameter space that has no valid value for M (the red hatched regions).

The low-energy SM running of α_s^{EFT} is fixed; so, to increase the value of M for a given set of initial UV couplings, we need α_s to run more strongly under the β functions of the full model. In general, increasing the field multiplicities will produce stronger running, as the coefficients of the terms in the β functions increase. Since we need the coefficients of the one-loop terms to be negative in order to have an IRFP, the strongest running will occur when the coefficient of the one-loop term is negative with a small magnitude, and the coefficients of the two-loop terms are positive with a larger magnitude.⁷ This also correlates with the IRFP couplings α_s^* and α_d^* having small values, as the β functions will be zero when, roughly, the one-loop coefficient $\times \alpha^2 \sim$ two-loop coefficient $\times \alpha^3$.

From Eq. (2), we see that increasing the multiplicities of the jointly charged fields— n_{f_j} and n_{s_j} —increases the coefficients of all terms in the β functions. Since n_{f_j} can be no larger than 3 in order to keep the one-loop terms negative, we consider models with larger n_{s_j} when searching for models with a larger new physics scale M . In particular, we look at all models with $n_{s_j} \geq 10$, where the maximum multiplicity for each field is given in Table II.

We note that in Table II there is only an upper limit on the total number of dark fermions n_{f_d} , and not on the specific multiplicities of the light and heavy dark fermions, $n_{f_{d,l}}$ and $n_{f_{d,h}}$; this is because the β functions of the full model only depend on n_{f_d} . The new physics scale M and the decoupling scale μ_0 also only depend on n_{f_d} , as they only depend upon the SM running of α_s in addition to the RGE evolution using the full β functions. So, for the purposes of searching for models with larger values of M , we only specify the value of n_{f_d} .

Using this definition of a model, there are 10 141 120 models for which $n_{s_j} > 10$, of which 120 015 have a perturbative fixed point. To have sufficiently strong running of the gauge couplings, we then look for models whose one-loop coefficients for the β functions are negative with a small magnitude, where we take that to mean that the coefficient is between -0.1 and 0 ; there are 188 such models. For all of these models, the scale of new physics M is greater than 1 TeV for at least 80% of the $\alpha_s^{\text{UV}} - \alpha_d^{\text{UV}}$ parameter space; that is, the value of M is large enough to avoid strict collider constraints in the majority of parameter space.

So, having found this set of models, we now wish to check which values of ϵ_v they can obtain. If we find models that have a decently large value of ϵ_v , and also have

⁷Note that although the magnitude of the one-loop term will be smaller than the two-loop terms, this is due to a cancellation between the matter terms and gluon terms in the one-loop coefficient. The individual one-loop terms will still be smaller than the individual two-loop terms for perturbative $\alpha < 0.3$, as discussed in Sec. VA.

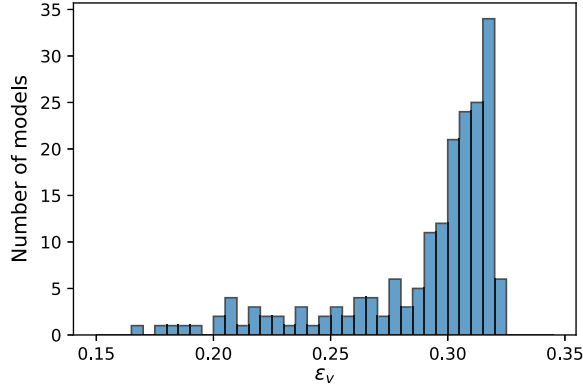


FIG. 9. A histogram of the validity fractions for the set of 188 models that have ten or more joint scalars, and one-loop coefficients for the β functions between -0.1 and 0 . Each of these models has a mass scale $M > 1$ TeV for at least 80% of the UV coupling parameter space.

sufficiently large new physics scales in the majority of parameter space, then these models could serve to naturally explain the cosmological coincidence problem.

For each of the 188 models, we only specify n_{f_d} ; so, for a given model we are free to choose $n_{f_{d,l}} \leq n_{f_d}$, setting $n_{f_{d,h}} = n_{f_d} - n_{f_{d,l}}$. We also ensure that $n_{f_{d,l}} > 0$ so that there is at least one light dark fermion species to confine into dark baryons.

The choice of $n_{f_{d,l}}$ will change the value of the dark confinement scale Λ_{dQCD} for a given pair of initial UV

couplings, as Λ_{dQCD} depends on the low-energy running of α_d below the decoupling scale. The Λ_{dQCD} contours, and thus the validity fraction ϵ_v , then also depend on $n_{f_{d,l}}$. So, for each of the 188 models, we choose $n_{f_{d,l}}$ such that the value of ϵ_v is maximized. We show these values of ϵ_v in Fig. 9.

Most of these models have values for ϵ_v above 0.3, with the largest values just over 0.32. We show four models with $\epsilon_v > 0.32$ in Fig. 10. While these values of ϵ_v are not quite as large as those for the best models in Sec. VI A, a validity fraction of ~ 0.3 still corresponds to a decent proportion of the initial UV coupling parameter space for which the dark confinement scale is on the order of the visible confinement scale. These models also have $M > 1$ TeV for every point in the viable region of parameter space, and so manage to potentially provide an explanation for the cosmological coincidence problem while avoiding stringent collider constraints.

VII. CONCLUSIONS

In this paper we reassessed the feasibility of explaining the cosmological coincidence problem by utilizing infrared fixed points in a dark QCD framework. In the original work of Bai and Schwaller, the confinement scales of dark and visible QCD are related by a dynamical mechanism depending only on the value of the gauge couplings at the IRFP and the mass scale of the new particle content introduced. We extended this framework by incorporating the dependence of these results on the initial values of the gauge couplings in the UV.

To assess whether models within this framework are able to explain the cosmological coincidence problem, we needed to carefully define our notion of how “naturally” a given model produces visible and dark confinement scales of similar orders of magnitude. With the dark confinement scale now depending on the initial UV couplings, we analyzed each model by looking at the proportion of UV coupling parameter space for which one obtains a valid value for the confinement scale, denoted as the “validity fraction” ϵ_v .

We began by looking at a limited set of models where we introduced at most three of each new field. Of these 12 288 models, 155 have a perturbative IRFP. The maximum validity fraction for these models is ~ 0.4 , and there are 12 with $\epsilon_v > 0.35$. The models with larger validity fractions generally have smaller IRFPs.

While these models have a decently sized proportion of UV coupling parameter space for which the dark and visible confinement scales are related, the scale of new physics is below 1 TeV for most of this parameter space. These new colored sub-TeV fields face strict collider constraints. To see if models in this framework can avoid these constraints, we identified a set of 188 models for which at least 80% of the UV coupling parameter space has $M > 1$ TeV; all these models have 10 or more scalars charged under both visible and dark QCD. Of these models, most have $\epsilon_v \sim 0.3$.

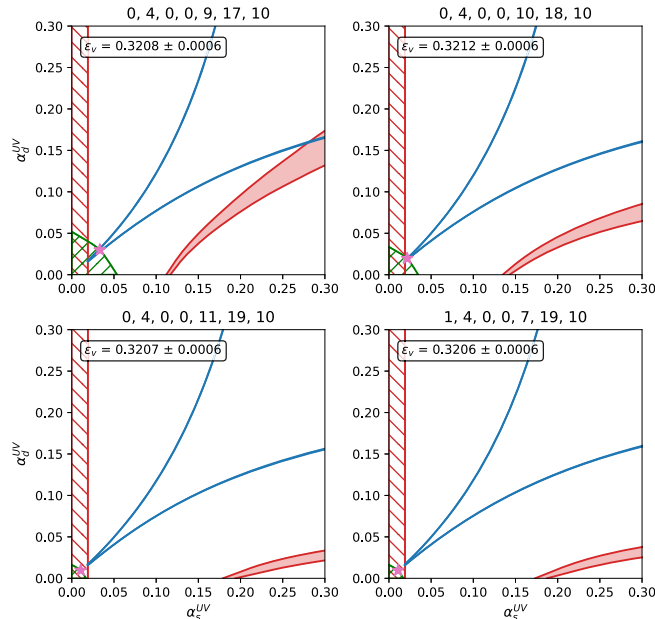


FIG. 10. Results for four models with $\epsilon_v > 0.32$. These are some of the models with the largest viability fraction in the set of 188 models shown in Fig. 9. The features of each subplot are the same as those in Fig. 6. Note that for each model, at least 80% of the parameter space has $M > 1$ TeV, where $M = 1$ TeV is shown by the red contour.

In conclusion, there do exist models within this framework that can potentially provide a natural explanation for the cosmological coincidence problem. While many of these models introduce new sub-TeV colored particles, there is a well-defined set of models that have a new physics mass scale high enough to avoid these collider constraints. In future work, these models could be candidates for more detailed model building, in order to incorporate a definite baryogenesis mechanism to generate the asymmetries in visible and dark matter, and to perform a proper phenomenological analysis.

ACKNOWLEDGMENTS

We would like to thank Jayden Newstead and Michael Schmidt for useful conversations. A. C. R. was supported by an Australian Government Research Training Program Scholarship. This research was supported by the Australian Government through the Australian Research Council Centre of Excellence for Dark Matter Particle Physics (CDM, CE200100008).

APPENDIX: BENCHMARK MODELS FROM BAI AND SCHWALLER

In Fig. 11 we plot the results for the seven benchmark models chosen by Bai and Schwaller. Table 2 of the original paper gives values of M and m_D (the dark baryon mass) for each model; in our analysis, these correspond to M and Λ_{dQCD} calculated for initial UV couplings at their IRFP values, $(\alpha_s^{\text{UV}}, \alpha_d^{\text{UV}}) = (\alpha_s^*, \alpha_d^*)$, and with $m_D \approx 1.5\Lambda_{\text{dQCD}}$. In Fig. 11, these are the values for M and Λ_{dQCD} at the point indicated by the pink star. We see that models C, E, and G have valid values of Λ_{dQCD} for initial UV couplings at their IRFP values; these correspond to dark baryon masses of 0.32, 3.5, and 1.2 GeV respectively. Most of the models have $\epsilon_v \sim 0.25$, with Model B having the largest validity fraction of $\epsilon_v = 0.300 \pm 0.009$. While this is a decently large validity fraction, as with the results in Sec. VI A, most of the valid region of parameter space for these models has a new physics scale below 1 TeV (the initial UV couplings that lie to the right of the red contour).

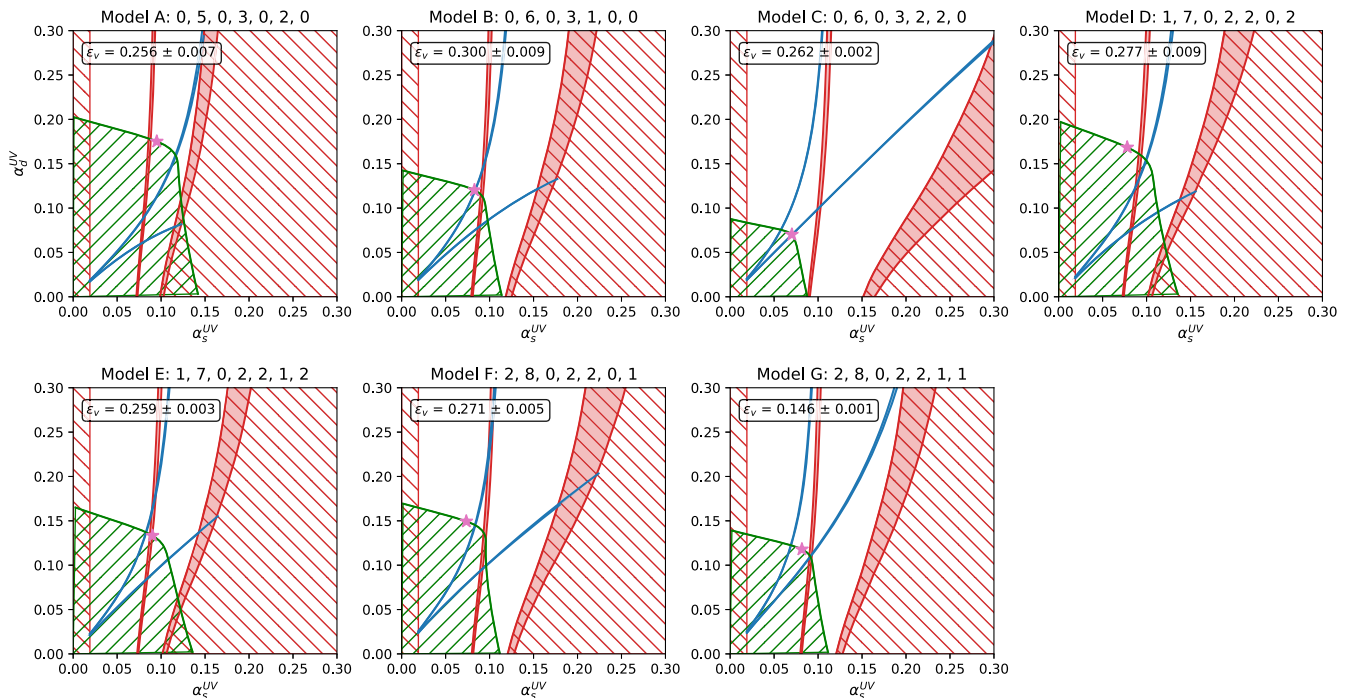


FIG. 11. Results for the seven benchmark models identified in the original paper by Bai and Schwaller. The features of each subplot are the same as those in Fig. 6. The results presented in the original paper correspond to our results when choosing the initial UV couplings to have their IRFP values (the point in each subplot identified by the pink star).

- [1] J. L. Feng, *Annu. Rev. Astron. Astrophys.* **48**, 495 (2010).
- [2] N. Aghanim *et al.* (Planck Collaboration), *Astron. Astrophys.* **641**, A6 (2020); **652**, C4(E) (2021).
- [3] K. Petraki and R. R. Volkas, *Int. J. Mod. Phys. A* **28**, 1330028 (2013).
- [4] K. M. Zurek, *Phys. Rep.* **537**, 91 (2014).
- [5] H. Hodges, *Phys. Rev. D* **47**, 456 (1993).
- [6] R. Foot and R. R. Volkas, *Phys. Rev. D* **68**, 021304 (2003).
- [7] R. Foot and R. R. Volkas, *Phys. Rev. D* **69**, 123510 (2004).
- [8] R. Foot, *Int. J. Mod. Phys. D* **13**, 2161 (2004).
- [9] M. Ibe, A. Kamada, S. Kobayashi, and W. Nakano, *J. High Energy Phys.* **11** (2018) 203.
- [10] H. An, S.-L. Chen, R. N. Mohapatra, and Y. Zhang, *J. High Energy Phys.* **03** (2010) 124.
- [11] J.-W. Cui, H.-J. He, L.-C. Lu, and F.-R. Yin, *Phys. Rev. D* **85**, 096003 (2012).
- [12] S. J. Lonsdale, *Phys. Rev. D* **91**, 125019 (2015).
- [13] M. Farina, *J. Cosmol. Astropart. Phys.* **11** (2015) 017.
- [14] I. Garcia Garcia, R. Lasenby, and J. March-Russell, *Phys. Rev. Lett.* **115**, 121801 (2015).
- [15] M. Farina, A. Monteux, and C. S. Shin, *Phys. Rev. D* **94**, 035017 (2016).
- [16] S. J. Lonsdale, M. Schroor, and R. R. Volkas, *Phys. Rev. D* **96**, 055027 (2017).
- [17] S. J. Lonsdale and R. R. Volkas, *Phys. Rev. D* **97**, 103510 (2018).
- [18] M. Ibe, A. Kamada, S. Kobayashi, T. Kuwahara, and W. Nakano, *Phys. Rev. D* **100**, 075022 (2019).
- [19] H. Beauchesne, *J. High Energy Phys.* **09** (2020) 048.
- [20] W.-Z. Feng and J.-H. Yu, *arXiv:2005.06471*.
- [21] A. C. Ritter and R. R. Volkas, *Phys. Rev. D* **104**, 035032 (2021).
- [22] M. Ibe, S. Kobayashi, and K. Watanabe, *J. High Energy Phys.* **07** (2021) 220.
- [23] C. Murgui and K. M. Zurek, *Phys. Rev. D* **105**, 095002 (2022).
- [24] Y. Bai and P. Schwaller, *Phys. Rev. D* **89**, 063522 (2014).
- [25] J. L. Newstead and R. H. TerBeek, *Phys. Rev. D* **90**, 074008 (2014).
- [26] T. Lee and C.-N. Yang, *Phys. Rev.* **104**, 254 (1956).
- [27] I. Kobzarev, L. Okun, and I. Pomeranchuk, *Sov. J. Nucl. Phys.* **3**, 837 (1966).
- [28] Z. G. Berezhiani, *Acta Phys. Pol. B* **27**, 1503 (1996).
- [29] S. I. Blinnikov and M. Yu. Khlopov, *Yad. Fiz.* **36**, 809 (1982) [*Sov. J. Nucl. Phys.* **36**, 472 (1982)].
- [30] R. Foot, H. Lew, and R. R. Volkas, *Phys. Lett. B* **272**, 67 (1991).
- [31] R. Foot, H. Lew, and R. Volkas, *Mod. Phys. Lett. A* **07**, 2567 (1992).
- [32] A. Y. Ignatiev and R. R. Volkas, *Phys. Rev. D* **68**, 023518 (2003).
- [33] R. Foot and R. R. Volkas, *Phys. Rev. D* **70**, 123508 (2004).
- [34] Z. Berezhiani, D. Comelli, and F. L. Villante, *Phys. Lett. B* **503**, 362 (2001).
- [35] Z. Chacko, H.-S. Goh, and R. Harnik, *Phys. Rev. Lett.* **96**, 231802 (2006).
- [36] D. R. T. Jones, *Phys. Rev. D* **25**, 581 (1982).
- [37] T. Banks and A. Zaks, *Nucl. Phys.* **B196**, 189 (1982).
- [38] P. A. Zyla *et al.* (Particle Data Group), *Prog. Theor. Exp. Phys.* **2020**, 083C01 (2020).
- [39] J. M. Cornwall, R. Jackiw, and E. Tomboulis, *Phys. Rev. D* **10**, 2428 (1974).
- [40] T. Appelquist and J. Carazzone, *Phys. Rev. D* **11**, 2856 (1975).
- [41] S. Weinberg, *Phys. Lett. B* **91B**, 51 (1980).
- [42] B. A. Ovrut and H. J. Schnitzer, *Phys. Lett.* **100B**, 403 (1981).
- [43] K. G. Chetyrkin, B. A. Kniehl, and M. Steinhauser, *Nucl. Phys.* **B510**, 61 (1998).
- [44] K. G. Chetyrkin, J. H. Kuhn, and C. Sturm, *Nucl. Phys.* **B744**, 121 (2006).
- [45] M. Davier, A. Hocker, and Z. Zhang, *Rev. Mod. Phys.* **78**, 1043 (2006).
- [46] S. J. Brodsky, G. P. Lepage, and P. B. Mackenzie, *Phys. Rev. D* **28**, 228 (1983).
- [47] F. A. Chishtie, *Front. Phys.* **9**, 765960 (2022).
- [48] P. M. Stevenson, *Phys. Rev. D* **23**, 2916 (1981).
- [49] S. Weinberg, in *14th International School of Subnuclear Physics: Understanding the Fundamental Constituents of Matter* (Springer, Boston, MA, 1976), 10.1007/978-1-4684-0931-4_1.
- [50] S. Weinberg, Ultraviolet divergences in quantum theories of gravitation, in *General Relativity: An Einstein Centenary Survey* (University Press, Cambridge, UK, 1980), pp. 790–831.